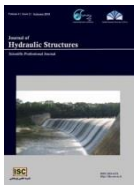
Journal of Hydraulic Structures
J. Hydraul. Struct., 2024; 10(1): 80-105
DOI: 10.22055/jhs.2024.46290.1290



OPEN ACCESS

Integrated Hydrodynamic Modeling of Dam Failure and Downstream Flood Inundation near Kathmandu, Nepal using MIKE Hydro River Model

Kuldeep Pareta[1]

Abstract

The integrated hydrodynamic modeling study conducted in the Kathmandu valley, Nepal, utilizing the MIKE Hydro River Model and incorporating diverse datasets, including satellite imageries, ALOS PALSAR RTC DEM data, topographical map at 1:25,000 scale and hydraulic data. Various scenarios, including a probable maximum flood (PMF) routing simulation, were examined, with a focus on assessing impacts on infrastructure, particularly two bridges located at different chainages. The analysis uncovered that the invert level at bridge-1 measured 1384.19 meters, while at bridge-2, it was recorded at 1343.98 meters. Historical records show significant floods in various years, including 1988, 1991, 1995, 1996, 1999, 2018, 2019, 2021, 2022, and 2023. During the flood inundation modeling, it was observed that the water level of the river near Gokarneshwar Mahadev and its adjacent areas experienced an elevation increase to 13 meters. Furthermore, the water level near both modeled bridges was noted to rise to 8 meters. Conversely, in other segments of the modeled river, the water level ranged between 5 to 6 meters. Hydrodynamic modeling emerged as a critical tool for flood risk assessment, providing accurate simulations of water flow behavior and facilitating informed decision-making for flood risk management and infrastructure resilience.

Keywords: Hydrodynamic modeling, dam failure, flood inundation, Kathmandu, MIKE Hydro River.

Received: 06 March 2024; Accepted: 02 April 2024

1. Introduction

Reservoir dams and water conservancy projects play a crucial role in providing various socio-economic benefits, including flood control, hydropower generation, irrigation, water supply, fisheries, and tourism [1]. However, the significant energy potential stored in reservoirs also poses a considerable risk to the safety of downstream communities and infrastructure [2-5]. Recent years

[1] DHI (India) Water & Environment Pvt Ltd., New Delhi, India. Email: kpareta13@gmail.com, kupa@dhigroup.com **(Corresponding author)**

CC BY

have witnessed a rise in the frequency of extreme climate events, which has raised concerns about the adequacy of existing flood control standards based on historical hydrological data [6, 7]. These climate extremes often result in prolonged operation of reservoir dams under unfavorable conditions, leading to increased stress on dam structures and accelerated degradation of hydraulic materials [8-11]. Consequently, the potential for dam failures is heightened, posing a severe threat to downstream areas [12-15]. Historical records of dam failures across different countries highlight the potential for catastrophic consequences, including loss of life and extensive damage to property downstream (Table 1). Dam failures can occur due to various factors such as floodwater infiltration, overtopping, material instability, or external damage [16-18]. The process of dam failure can vary, ranging from gradual deterioration to sudden, catastrophic collapse [19-21]. The nature of dam failure significantly influences the flood dynamics and downstream impacts, which can vary in terms of severity and extent [22-24].

Table 1. List of historical records of dam failures across different countries

Date	Location	Casualty	Details
1894-08-25	Gohna lake dam (Garhwal, India)	3	A landslide dam failed after authorities successfully evacuated the valley [25].
1917-08-19	Tigra dam (Gwalior, India)	1 000	Failure due to water seepage through sandstone foundation, potentially leading to increased casualties [26].
1928-03-12	St. Francis dam (Santa Clarita, California, US)	431	Dam failure attributed to geological instability of east canyon wall. Possible unreported casualties due to undocumented migrant workers below [27].
1943-05-17	Möhne dam (Ruhr, Germany)	1 579	Destroyed by bombing during World War II operation. Eleven factories destroyed, 114 seriously damaged [28].
1959-12-02	Malpasset dam (Côte d'Azur, France)	423	Geological fault possibly enhanced by explosives work during construction; initial geo-study was not thorough. Two villages were destroyed [29].
1961-07-12	Panshet dam (Pune, India)[2]	1,000	Dam wall burst under rainwater pressure. Concrete blocks substituted for steel-reinforced concrete due to steel scarcity [30].
1963-10-09	Vajont dam (Monte Toc, Italy)	2 000	Reservoir filling triggered valley wall geological failure, causing a 110 km/h landslide into the lake. Water overflowed dam in a wave. Misjudged valley stability led to village devastation [31].
1965-03-28	El Cobre new and old dam (Valparaíso, Chile)	400	Earthquake-induced liquefaction led to the release of water and mining waste, burying El Cobre town downstream [32].
1972-06-09	Canyon lake dam (South Dakota, United States)	238	Debris-clogged dam outlets resulted in flooding, causing 3,057 injuries and destruction of over 1,335 homes and 5,000 automobiles [33].
1975-08-08	Banqiao and Shimantan dams	26,000	Extreme rainfall from Typhoon Nina exceeded the dam's design capacity, leading to its failure.

[2]July 12, 1961 Lest We Forget. sakaaltimes.com. Archived from the original on 1 April 2016. Retrieved 6th March 2024.

	(Zhumadian, China)		Eleven million people lost their homes. The dam was reconstructed between 1986 and 1993 [34].
1976-06-05	Teton dam (Idaho, United States)	11	Geological issues, including unsuitable bedrock, seismic activity, and caves, contributed to the dam failure. Water leakage eroded the earthen wall, leading to the collapse. Thirteen thousand head of cattle died as a result [35, 36].
1979-08-11	Machchu-2 dam (Morbi, India)	5,000	Intense rainfall led to observed flow reaching 16307 m^3/s, three times the dam's design capacity, causing its collapse. The dam embankment, measuring 762 meters on the left and 365 meters on the right, collapsed. Floods, reaching heights of 3.6 to 9.1 meter, inundated low-lying areas of Morbi industrial town within 20 minutes [37].
1985-07-19	Val di Stava dam (Tesero, Italy)	268	Inadequate maintenance and narrow design margins resulted in outlet pipe failure, exerting pressure on the dam [38, 39].
2008-08-18	Koshi barrage (Koshi Zone, Nepal/India)	250	Failure to maintain the barrage coupled with weak monsoon and preceding drought led to its collapse, affecting 2.3 million people in northern Bihar [40, 41].
2013-06-17	Chorabari lake (Kedarnath, Uttarakhand, India)	10,000	Intense rainfall led to flash floods and the breach of Chorabari Lake Kedarnath in Uttarakhand, resulting in widespread devastation and loss of life [42, 43, 44].
2018-07-11	Panjshir valley dam (Panjshir Valley, Afghanistan)	10	A deteriorated dam collapsed during heavy summer rainfall, causing 13 individuals to go missing and destroying 300 houses [45].
2019-01-25	Brumadinho dam (Minas Gerais, Brazil)	270	A catastrophic failure of a tailings dam released 12 million cubic meters of tailings slurry [46, 47].
2019-07-02	Tiware dam (Ratnagiri, India)	23	Heavy rains led to the overtopping and breaching of the dam [48].
2021-02-07	Uttarakhand flood (Chamoli, Uttarkhand, India)	61	The Rishi Ganga dam was destroyed by an avalanche or glacier burst, causing a surge of water downstream and breaching the Tapovan Hydropower Plant, with 145 people reported missing [49].
2023-09-11	Derna dam collapses (Derna, Libya)	20,000	Two dams, approximately 75 and 45 meters tall, failed due to heavy rain from Storm Daniel during the Libyan civil war, inundating the city of Derna with around 30 MCM of water [50].

Given the significant risks posed by dam failures and subsequent floods, there is a critical need for comprehensive hydrodynamic modeling and mapping studies to assess and mitigate these risks effectively. This paper presents a hydrodynamic numerical modeling approach utilizing the MIKE Hydro River Model to simulate dam failure scenarios and downstream flood inundation near Kathmandu metropolitan city, Nepal. This study offers significant contributions by generating comprehensive flood inundation maps, which serve as vital tools for emergency preparedness, land-use planning, and infrastructure development initiatives. Furthermore, the insights derived

from this research can inform policy decisions aimed at bolstering dam safety protocols and resilience strategies, particularly in light of evolving climatic conditions. However, it is crucial to recognize the inherent limitations of hydrodynamic modeling, which encompass uncertainties related to input data, model assumptions, and simplifications. Despite these challenges, the study provides valuable insights into the understanding and mitigation of dam failure risks and downstream flood hazards in the Kathmandu region, thereby fostering greater resilience among local communities in the face of water-related disasters.

Additionally, the flood mapping process incorporated considerations for factors such as topography, land use, and infrastructure to accurately depict the extent of flooding. The resulting flood inundation maps provided valuable information for assessing flood risk, identifying vulnerable areas, and informing disaster management and mitigation efforts in the Kathmandu region of Nepal. The river, a significant watercourse in Kathmandu metropolitan city, has been notorious for causing recurrent floods, necessitating the urgent need for flood mapping initiatives. Historical records indicate notable flood events attributed to this river occurring in various years, including 1988, 1991, 1995, 1996, 1999, 2018, 2019, 2021, 2022, and 2023. These flood incidents have posed significant challenges to the inhabitants and infrastructure of Kathmandu metropolitan city, highlighting the importance of comprehensive flood mapping studies to understand the spatial extent, severity, and frequency of flooding along the river.

The primary objectives of this investigation are as follows: (i) to quantify the maximum probable inflow hydrograph into the reservoir utilizing the MIKE Hydro River model; (ii) to explore potential dam failure scenarios; and (iii) to generate predictive inundation maps for the studied basin in response to dam breach events.

The following sections represent a comprehensive literature review of previous dam failure modelling to discern and analyze the latest methodologies employed in research conducted by various authors worldwide. This analysis aids in the selection of an appropriate methodology and numerical model for conducting dam failure study.

Johnson et al. [51] proposed breach shapes for earthen, gravity, and arch dams. They found that earthen dams commonly exhibit a trapezoidal breach shape, with occasional instances of triangular breaches. Singh et al. [52] found that breach widths ranged from 2 to 5 times the dam height in 20 dam failures. The time to complete failure was typically 0.25 to 1 hour. Maximum overtopping depths before failure ranged from 0.15 to 0.61 meters for overtopping failures. MacDonald et al. [53] proposed a breach formation factor, linking outflow volume and water depth at failure. They associated embankment material removal with this factor across dam types. Most breaches had 1h:2v slopes, triangular or trapezoidal shapes, based on depth. An envelope curve for breach formation time versus eroded material volume was suggested for earth fill dams, while non-earth fill dam failures were less predictable due to structural instabilities. Petra et al. [54] showed that breach width and formation time significantly affect discharge, inundation levels, and flood arrival time near the dam. Downstream, breach formation time alters flood peak timing, but peak discharge and inundation levels remain relatively insensitive. Singh et al. [55] compared DAMBRK and HEC-1 for eight breached dams, varying breach parameters to predict peak outflows. Larger reservoirs showed larger peak outflow changes (35-87%) with breach width (BW) variations, while smaller reservoirs exhibited smaller changes (6-50%).

Froehlich [56] developed non-dimensional equations to predict breach width, side-slope factor, and breach formation time based on dam characteristics. Results indicated wider breaches and faster lateral erosion for overtopping-induced failures compared to other causes. Wurbs [57] identified breach simulation as the most uncertain aspect of dam-breach flood wave modeling. In large reservoirs, peak discharge correlates with breach dimensions, while accurate breach

geometry prediction is crucial. In small reservoirs, peak outflow precedes complete breach development, emphasizing the importance of breach formation rate. Singh et al. [58] analyzed breach geometry and failure times from 52 case studies. They found Btop/Bbottom ratio ranging from 1.06 to 1.74, with an average of 1.29. Breach side slopes were typically 10-50°. Most failure times were under 3 hours, with 50% under 1.5 hours. Von Thun et al. [59] and Dewey et al. [60] used data from previous studies to propose guidance for estimating breach parameters. They suggested 1:1 side slope, except for dams with cohesive shells or wide cores, where 1:2 or 1:3 slopes may be suitable.

Horritt et al. [61] evaluated 1D and 2D flood models HEC-RAS, LISFLOOD-FP, and TELEMAC-2D on a 60 km stretch of the River Severn, UK. Using radar remote sensing data, they calibrated models with floodplain and channel friction parameters, finding HEC-RAS and TELEMAC-2D reliable with observed data, while LISFLOOD-FP required calibration against inundated area. Merritt et al. [62] evaluated empirical, conceptual, and physical models for sediment generation and transport processes. They found that empirical and simple conceptual models are suitable for limited input data and computational simplicity, while physical models are data-intensive and complex, posing challenges in areas with limited data availability. Yang et al. [63] developed a direct processing approach for river floodplain delineation using GIS integration with HEC-RAS. They simulated water surface profiles for various storm events and validated the model using a 100-year flood zone. The study emphasizes integrating hydraulic data with GIS for floodplain mapping. Bani Hashemi et al. [64] applied a 2D dam failure model based on Fred and Mac Cormac, enhancing it with second-order accuracy and artificial viscosity. This combination effectively simulated gradual dam failure and shock flow resolution despite its simplicity. Montazeri Naming et al. [65] developed one and two-dimensional numerical models to simulate the wave of Maronik Dam failure and subsequent flooding.

Abareshi et al. [66] assessed the risks associated with Taragh concrete dam failure near Mashhad city using MIKE 11 software. They identified flood-prone areas by combining flood speed and depth maps through a risk matrix, determining risk rates for each area. Esmaili et al. [67] used Fluent software to model hydraulic failure of a dam caused by sudden floods. Their one-dimensional study explored two scenarios: flood and failure, and failure without flood. Results emphasized the significance of the applied network over the time step in influencing outcomes. Ahmadi [68] numerically modeled gradual dam failure, initiating erosion with an initial gap on the crown. Model results were compared with laboratory and field test results, showing relatively good consistency through provided charts. Timbadiya et al. [69] created a hydrodynamic model of the lower Tapi River with HEC-RAS for unsteady flow conditions using surveyed stream data and boundary conditions. Simulated floods closely matched observed flows at various stations, validating the model for flood forecasting in the lower Tapi River. Godariz et al. [70] analyzed the risk of earth dam failure caused by body overflow considering uncertain input parameters. Nejad et al.[71] simulated dam failure and wave propagation using a limited volume numerical method in two dimensions. Seiyfi Zade et al. [72] investigated PolRud dam failure due to breach and flood routing downstream using the BREACH GUI model. Flood effects analyzed with the HEC-RAS model for determining dam failure impacts.

Aureli et al. [73] assessed hydrodynamic forces on dams leading to failure with 2D and 3D models, combining experimental and numerical approaches. Kocaman et al. [74] explored dam failure due to shock waves impacting a vertical wall using empirical testing and computational fluid dynamics (CFD) simulations with the Volume of Fluid (VOF) method. Wood et al. [75] investigated dam failure flows in canals with a 90-degree bend using experimental and numerical methods. The study employed 2-dimensional equations, specifically the Shallow Water Equations

(SWE). Dottori et al. [76] developed high-resolution flood hazard models using daily river discharge data from the Global Flood Awareness System (GloFAS). They evaluated flood hazard maps for different return periods globally, comparing them with official flood maps and studying model sensitivity and limitations. Vermee et al. [77] developed a dam break flow simulation model for Bargi Dam on the Narmada River near Jabalpur. The study focused on overtopping failure of the earthen part, examining its impact on Narmada River, Jabalpur city, and presenting inundation maps using MIKE11-DB.

Palu MC et al. [78] improved 1D routing algorithms for dam-break floods. Classical models showed errors up to ~18% in peak discharge prediction and up to 4-hour differences in peak timing. Their modified approach, using a linear diffusive wave format, reduced errors to less than -0.1% in peak discharge prediction. Li et al. [79] conducted a sensitivity analysis on rock-fill dam break floods for different durations. They found that longer durations decrease peak discharge, extend flood appearance time, and lower water levels downstream. This research aids in optimizing dam design and flood countermeasures. Adityawan et al. [80] conducted numerical modeling of dam break flow through urban areas, comparing three approaches for defining buildings: wall boundary, contour, and Manning. They found the wall boundary approach to be most accurate, recommending it for buildings without height variation or submergence. Annunziato et al. [81] developed a rapid procedure for assessing the consequences of dam break events using the shallow water model NAMI DANCE. This allows quick generation of input decks and output quantities, facilitating fast analysis of flood risk. The method can be integrated into systems like GDACS for timely flood alerts.

2. Methodology

2.1. About the study area

The study area is situated near Kathmandu, Nepal, focusing on the river passing through the Kathmandu metropolitan city and a dam located at the upstream of the city (Figure 1). The study area exhibits a heterogeneous topography, featuring a combination of elevated terrain characterized by hills and low-lying regions represented by valleys. This varied landscape configuration significantly influences the hydrological dynamics within the region. The river network serves as a fundamental component of the local hydrology, functioning as the primary conduit for water flow and distribution throughout the Kathmandu valley. Moreover, the presence of a dam situated upstream of Kathmandu significantly contributes to the management of the region's water resources and the implementation of flood control measures. However, the area's distinctive geographical attributes, coupled with the ongoing processes of urbanization and infrastructural expansion, pose formidable challenges for the accurate modeling of hydrodynamic processes associated with dam failure and subsequent flood inundation events.

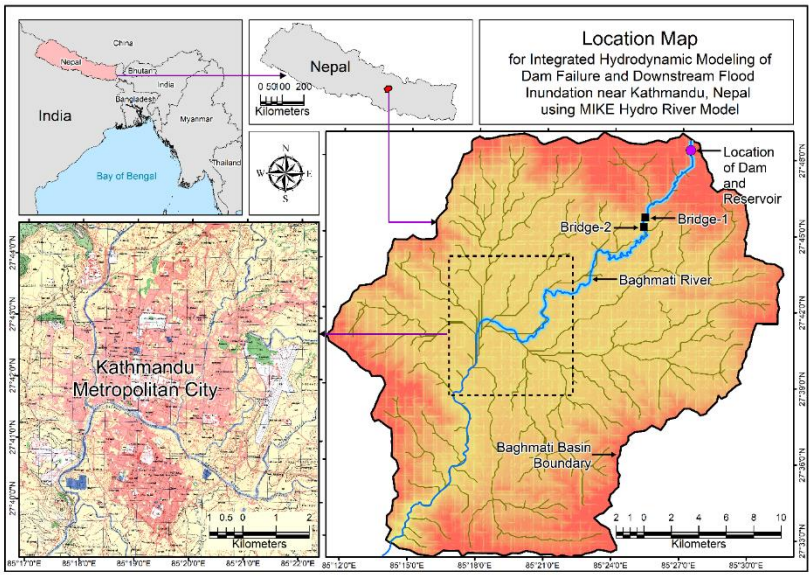


Figure 1. Location map of the study area.

2.2. Data collection

Data collection involved gathering topographic, hydrological, and hydraulic information, including digital elevation models (DEMs), river cross-section data, and reservoir characteristics. The study area's diverse terrain, including steep slopes and complex river networks, posed challenges for accurate modeling. MIKE Hydro River Model facilitated comprehensive analysis by integrating various datasets, enabling a detailed assessment of flood dynamics and inundation extents.

Landsat-9 OLI-2 satellite imagery, characterized by a spatial resolution of 30 meters, was sourced from the USGS Earth Explorer database, dated 14th May 2023. Subsequently, a fusion process was employed to integrate the G-R-NIR bands (30 meters), with the PAN band (15 meters). This fusion technique aimed to enhance the overall spatial resolution of the imagery. The resultant satellite data, thus augmented, facilitated the extraction of general features and Land Use/Land Cover (LULC) information within the study area. Specifically, the LULC data derived from this imagery served as a basis for determining Manning (M) coefficients utilized in the hydrodynamic modeling of the study area.

Sentinel-2 satellite imagery with a spatial resolution of 10 meters, acquired on 23rd May 2023, was procured from the European Space Agency's Copernicus Programme via the Sentinels Scientific Data Hub. This satellite data served as a critical resource for validating the observed flood event against the inundation map predicted by the hydrodynamic model. Through comparative analysis, the accuracy and reliability of the model's predictions were assessed, contributing to the validation and refinement of the flood inundation mapping process.

ALOS PALSAR (radiometric terrain correction) DEM data with a spatial resolution of 12.5 meters, was obtained from the Alaska Satellite Facility (ASF) via Vertex. This high-resolution DEM data facilitated the analysis of the general topography within the study area, enabling the extraction of cross-sectional profiles of the river. The drainage network and basin boundary of the study area were derived from the DEM data as well.

A topographical map, designated as Sheet No. 2785 06A and scaled at 1:25,000, was acquired from the Survey Department, Government of Nepal. This map served as a foundational resource

for the study, facilitating the overlay of flood inundation data to assess the extent of settlement flooding. Additionally, Google Earth satellite imagery was leveraged for comparative analysis and validation of the observed flood inundation patterns. These mapping resources provided essential spatial context and reference points for accurately depicting and analyzing the impacts of flooding on the surrounding landscape and settlements.

Hydrological and hydraulic data, including stage-discharge relations, area-elevation curves of reservoirs, rating curves of spillways, and probable maximum flood information, were sourced from the Department of Hydrology and Meteorology (DHM), Government of Nepal. These datasets were obtained from the DHM's repository. They played a crucial role in defining the boundary conditions of the hydrodynamic model. By utilizing these datasets, accurate representations of the river system's behavior and response to various scenarios were established, enhancing the reliability and validity of the model simulations.

2.3. Component of MIKE Hydro River for dam failure

In the dam failure analysis conducted using the MIKE Hydro River Model, a schematic diagram of the river and reservoir system is essential for accurately simulating the flood inundation dynamics. This schematic diagram encompasses various elements, including the river channel, hydraulic structures such as dams and spillways, and the reservoir area upstream of the dam. Additionally, it incorporates topographic features such as elevation contours and land use/land cover information to capture the spatial distribution of floodwaters. The reservoir model accounts for the storage capacity of the reservoir and the inflow-outflow dynamics, while the river model represents the hydraulic behavior of the river channel and floodplain areas (Figure 2). By integrating these components into a coherent schematic diagram, the MIKE Hydro River Model enables researchers and practitioners to simulate dam failure scenarios with high fidelity, providing valuable insights into flood inundation extent, depth, and propagation patterns for effective flood risk assessment and management.

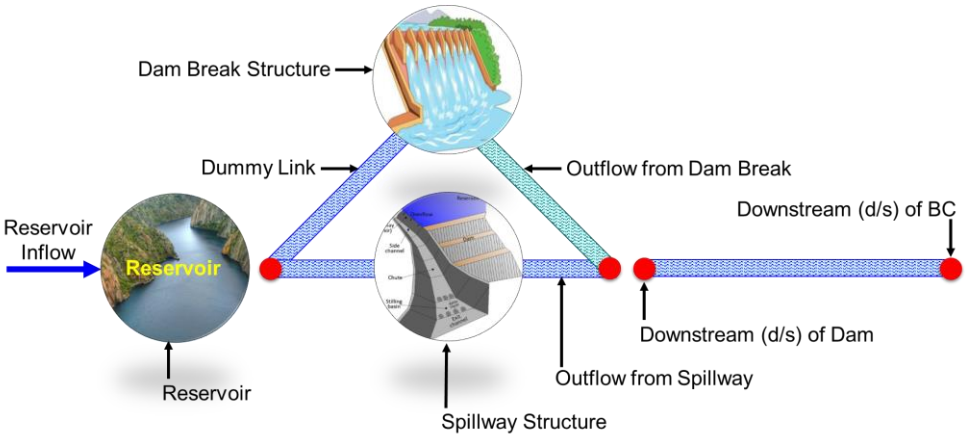


Figure 2. Schematic diagram of MIKE Model for dam failure modelling [82].

2.4. Dam breach parameters

The estimation of dam failure flood characteristics relies on several key parameters related to the dam breach process. These parameters include the initial and final breach width, the shape of the breach, the duration of breach development, and the reservoir level at the onset of breach

initiation. The mechanism governing breach formation predominantly hinges on the type of dam and the underlying cause of dam failure. These factors collectively determine the dynamics of the breach and subsequent flood inundation, highlighting the importance of accurately defining these parameters in dam failure modeling for effective risk assessment and mitigation strategies. The graphical representation of the physical parameters is depicted in Figure 3, providing a visual summary of the key characteristics.

The breach depth, alternatively termed breach height in certain literature, denotes the vertical dimension of the breach, extending from the crest of the dam to the invert of the breach. In certain instances, publications may specify the reservoir head at the breach, measured from the surface level of the reservoir to the breach invert.

The breach width, a critical parameter in dam failure analysis, significantly influences the peak flow rate and subsequent inundation levels downstream. Studies often document either the mean breach width or specify measurements at both the top and bottom of the breach aperture.

The breach side slope factor, in conjunction with breach width and depth, delineates the geometric configuration of the breach aperture. While crucial, precise estimation of breach side slope angles typically assumes lesser significance compared to accurately predicting breach width and depth.

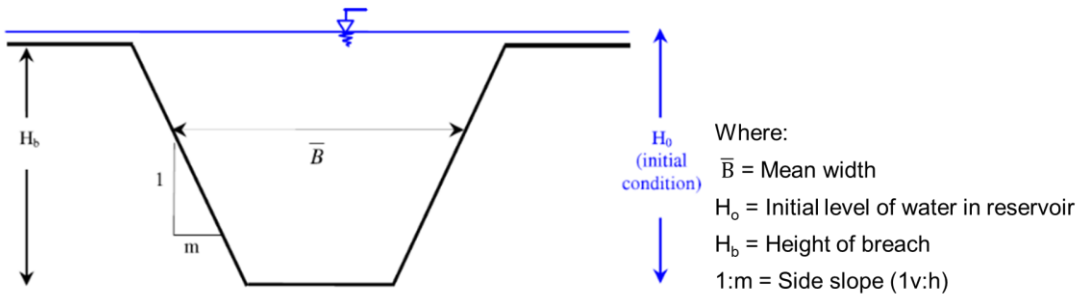


Figure 3. Final dimension of a trapezoidal dam breach approximation

Research on various dam failures suggests that failures in Concrete-Faced Rockfill Dams (CFRDs) often occur due to slumping of the embankment shoulders, resulting in overtopping. Additionally, issues such as cracking and internal erosion of the abutments during initial reservoir filling may lead to piping failures caused by seepage. Furthermore, failure of the spillway can contribute to erosion of the downstream shoulder.

2.4.1. Review of guidance for breach parameters

Several governmental bodies have released regulatory frameworks outlining potential ranges for breach parameters such as width, side slopes, and development time. A comprehensive overview of this guidance is presented in Table 2.

Table 2. Ranges of Possible Values for Breach Characteristics [83].

Dam Type	Average Breach Width (B_{avg})	Horizontal component of breach side slope (H)	Failure time (t_f) in hrs.	References
Earthen / rockfill	(0.5 to 3.0) x HD	0 to 1	0.5 to 4.0	HEC [84]
	(0.5 to 5.0) x HD	0 to 1	0.1 to 4.0*	USACE [85]
	(1.0 to 5.0) x HD	0 to 1	0.1 to 1.0	FERC [86]
	(2.0 to 5.0) x HD	0 to 1 (slightly larger)	0.1 to 1.0	NWS [87]
Concrete gravity	Multiple Monoliths	Vertical	0.1 to 0.5	USACE [85]
	Usually, ≤ 0.5 L	Vertical	0.1 to 0.3	FERC [86]
	Usually, ≤ 0.5 L	Vertical	0.1 to 0.2	NWS [87]
Concrete arch	Entire Dam	Valley wall slope	≤ 0.1	HEC [84]
	(0.8 x L) to L	0 to valley walls	≤ 0.1	USACE [85]
	Entire Dam	0 to valley walls	≤ 0.1	FERC [86]
	(0.8 x L) to L	0 to valley walls	≤ 0.1	NWS [87]
Slag / refuse	(0.8 x L) to L	1.0 to 2.0	0.1 to 0.3	FERC [86]
	(0.8 x L) to L		≤ 0.1	NWS [87]
Where:	*HD = Height of the dam. L = Length of the dam crest*			
** Note*	*Dams characterized by extensive water volumes and extended crest lengths are prone to sustained erosion over prolonged periods, contingent upon the ongoing flow of a substantial water volume through the breach. Consequently, such dams may exhibit broader breach widths and protracted breach development times compared to documented cases.*			

2.4.2. Regression Equations

The regression equations delineated herein have been employed across various dam safety investigations documented in the literature and are under contemplation for integration into the guidance framework for the Portfolio Risk Assessment study conducted by the Corps of Engineers: (i) Froehlich [56, 88, 89]; (ii) MacDonald et al. [53]; and (iii) Von Thun et al. [59].

Froehlich equation [56, 88, 89] conducted an analysis incorporating 63 datasets pertaining to various dam types, including earthen, zoned earthen, earthen dams with a core wall (i.e., clay), and rockfill dams. The study aimed to derive equations for estimating average breach width, side slopes, and failure time. In the application of these equations, it was assumed that the breach extends from the crest of the dam to the natural ground elevation at the centerline of the breach location. The empirical equation is:

$$B_{avg} = 0{,}1803 K_0 V_w^{0,32} h_b^{0,19}$$
$$t_f = 0{,}00254 (V_w)^{0,53} h_b^{-0,9}$$

MacDonald and Langridge-Monopolis equation [53] conducted an analysis using 42 datasets primarily comprising earthfill, earthfill with a clay core, and rockfill dams. They aimed to establish a relationship known as the "Breach Formation Factor," which is the product of the volume of water released from the dam (V_{out}) and the water height above the dam. This factor was correlated with the volume of material eroded from the dam's embankment. The parameter V_{out}, representing the water volume passing through the breach, is typically unknown prior to breach analysis and is initially estimated as the reservoir water volume at breach initiation. Subsequently, after performing breach analysis and obtaining a better estimate of the actual water volume passing through the breach, parameters can be recalculated iteratively. The empirical equation is:

$$V_{er} = 0{,}0261 (V_w h_w)^{0,769}$$ for earthfill

$V_{er} = 0{,}00348(V_w h_w)^{0{,}852}$ for noneartfill
$t_f = 0{,}0179 V_{er}^{0{,}364}$

Von Thun and Gillette equation [59] analyzed data from 57 dams sourced from [56] [53]. Their methodology proposes breach side slopes typically set at 1.0H:1.0V, with exceptions for dams with cohesive soils, where slopes range from 0.5H:1V to 0.33H:1V. They formulated two sets of equations to estimate breach development time, contingent on the embankment material. The empirical equation is:

$B_{avg} = 2{,}5h_w + C_b$
$C_b = 54.9$ for b_w for reservoir storage greater than 12.8 Mcum
$t_f = 0{,}015h_w$ highly erodible
$t_f = 0{,}020h_w + 0{,}25$ erosion resistant

Breach parameters: In the current study, the initiation point, and initial breach level correspond to the crest level of the breaching section and the riverbed level, respectively. A sensitivity analysis was conducted, varying breach width, breach time, and breach slope. The breach parameters outlined in Table 3 were chosen for the dam failure investigation.

Table 3. Breach parameter for investigative dam.

Average breach width (m)	Time of failure (hr)	Slope (H)	Breach level (m)		Remarks
			Initial	Final	
20	0.5 1 2 4	0.5	2095.5	2076	Scenario-1
30	0.5 1 2 4	1.0	2095.5	2076	Scenario-2
45	0.5 1 2 4		2095.5	2076	Scenario-3

2.5. Model setup MIKE Hydro River HD Model

The MIKE Hydro River HD Model was configured to simulate dam failure and subsequent flood inundation near Kathmandu, Nepal. The model setup involved defining the hydraulic characteristics of the river, dam, and reservoir. Detailed topographic and bathymetric data were incorporated to accurately represent the river and reservoir geometry. Boundary conditions such as upstream flow conditions and downstream water levels were specified to mimic real-world scenarios. The model was calibrated and validated using observed data to ensure its accuracy in predicting river flow and flood inundation extents. Additionally, the dam failure parameters obtained from sensitivity analysis were integrated into the model setup to simulate various dam failure scenarios.

2.5.1. River network and topography

The network comprises the reservoir of the dam and the river downstream of the dam. Figure 4 illustrates the network layout, including the precise positioning of the dam and bridges. The reservoir extends over a length of 688 meters, while the river spans a length of 33.7 km. The river is discretized into 241 cross-sections spaced at regular intervals along its length. This comprehensive representation of the network's geometry and hydraulic properties ensures accurate modeling of dam failure and flood inundation dynamics.

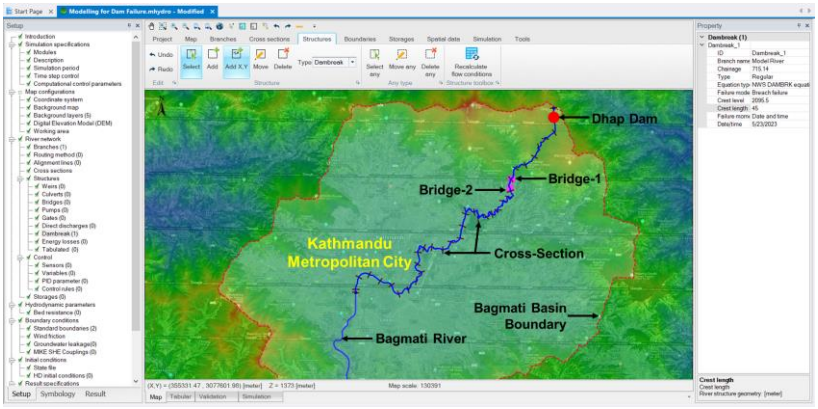


Figure 4. MIKE Hydro River model setup for dam failure analysis

2.5.2. Reservoir and dam

In the model, the reservoir is depicted through a distinct reservoir branch, with its elevation-surface area relationship delineated at chainage "0" km of the reservoir branch. The corresponding data detailing this relationship is provided in Table 4. This approach ensures that the reservoir's behavior and characteristics are accurately captured within the modeling framework, facilitating a comprehensive analysis of dam failure and subsequent flood inundation dynamics.

Table 4. Area-elevation curve of reservoir

Elevation (m)	Surface Area (m^2)	Elevation (m)	Surface Area (m^2)	Elevation (m)	Surface Area (m^2)	Elevation (m)	Surface Area (m^2)
2075.86	0.00	2081.00	11136.94	2086.50	62322.90	2092.00	111108.90
2076.00	3.32	2081.50	12971.78	2087.00	67495.95	2092.50	115406.83
2076.50	515.27	2082.00	15041.71	2087.50	73011.19	2093.00	119612.97
2077.00	867.48	2082.50	16454.74	2088.00	78883.13	2093.50	123815.64
2077.50	1260.03	2083.00	17902.54	2088.50	83203.16	2094.00	128015.24
2078.00	1686.16	2083.50	19388.34	2089.00	87406.61	2094.50	132793.17
2078.50	2182.52	2084.00	20912.66	2089.50	91529.07	2095.00	137438.62
2079.00	2797.87	2084.50	23143.60	2090.00	95544.41	2095.50	142125.02
2079.50	3558.56	2085.00	26681.10	2090.50	99409.71		
2080.00	4451.89	2085.50	31702.84	2091.00	103246.60		
2080.50	9533.45	2086.00	57547.00	2091.50	107146.14		

2.5.3. Spillway

In the model, the spillway is represented as an overflow weir, designed to manage excess water flow from the reservoir. This hydraulic structure plays a crucial role in controlling the water level within the reservoir and preventing overtopping during periods of high inflow. The spillway's hydraulic performance is characterized by its rating curve, which delineates the relationship

between the water level in the reservoir and the corresponding discharge through the spillway. This rating curve provides crucial information for accurately simulating the spillway's behavior under varying hydrological conditions (Figure 5 (A)). This information is vital for effectively modeling the spillway's operation and assessing its capacity to handle potential flood events. By incorporating the spillway's characteristics into the model, researchers can simulate various scenarios and evaluate the spillway's performance in mitigating flood risks and safeguarding downstream areas from potential inundation.

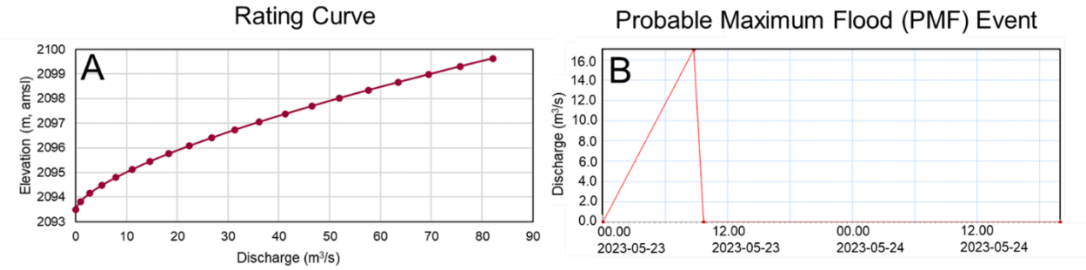


Figure 5. (A) Rating curve of spillway, (B) Probable Maximum Flood (PMF) used as U/S boundary condition

2.5.4. Boundary condition

In the MIKE Hydro River Model for dam failure analysis, boundary conditions play a crucial role in defining the hydraulic behavior of the river system [90]. At the upstream boundary, the Probable Maximum Flood (PMF) is employed as the boundary condition. The PMF represents the extreme flood event that could potentially occur in the upstream catchment area, thus providing a rigorous test of the dam's resilience to severe flooding scenarios. PMF shown in Figure 5 (B) is used as upstream boundary condition.

Conversely, at the downstream boundary of the river model, the boundary condition is defined by a stage-discharge relation. This relation specifies the relationship between the water level (stage) in the river and the corresponding discharge rate. By incorporating the stage-discharge relation at the downstream boundary, the model can accurately simulate the outflow from the river system under varying hydraulic conditions.

The downstream boundary condition for dam failure analysis is derived from Manning's equation. By applying Manning's equation, the stage-discharge relation establishes the correlation between the water stage (depth) in the river and the corresponding discharge rate. Table 5 provides the stage-discharge relation, delineating specific water stage levels and their corresponding discharge rates for the downstream boundary of the river model.

Table 5. Stage-discharge relation used as downstream boundary condition.

Stage (m, amsl)	Discharge (m^3/s)	Stage (m, amsl)	Discharge (m^3/s)	Stage (m, amsl)	Discharge (m^3/s)	Stage (m, amsl)	Discharge (m^3/s)
1277.56	0.00	1279.25	26.61	1280.94	177.56	1282.62	478.63
1277.90	0.65	1279.59	44.57	1281.27	226.10	1282.96	556.18
1278.24	3.34	1279.92	68.92	1281.61	280.55	1283.30	639.52
1278.57	8.22	1280.26	98.99	1281.95	340.80	1283.64	728.33
1278.91	15.36	1280.60	135.12	1282.29	406.84	1283.97	824.37

2.6. Critical condition for dam failure study

In the dam failure study, a critical scenario occurs when the reservoir is at its full reservoir level (FRL) and subjected to the probable maximum flood (PMF) hydrograph. In this study, the initial step involved reservoir routing by introducing the PMF into the reservoir while considering the water level at the FRL of 2093.5 m and assuming full openness of the spillway gates. The reservoir routing analysis revealed that the maximum water level reached was 2093.81 m, occurring one hour after the application of the PMF. The time series data illustrating the variation in reservoir level during the routing of the PMF is depicted in Figure 6. As the top of the dam is situated at an elevation of 2095.5 m, there is no overtopping of the dam anticipated. Consequently, for the hypothetical scenario of simulating a dam breach and to ascertain the maximum flood peak resulting from the breach, it is deemed appropriate to initiate the breach when the reservoir level reaches elevation 2093.81 m. This approach ensures a comprehensive assessment of the dam failure scenario and facilitates the determination of peak flood magnitudes accurately.

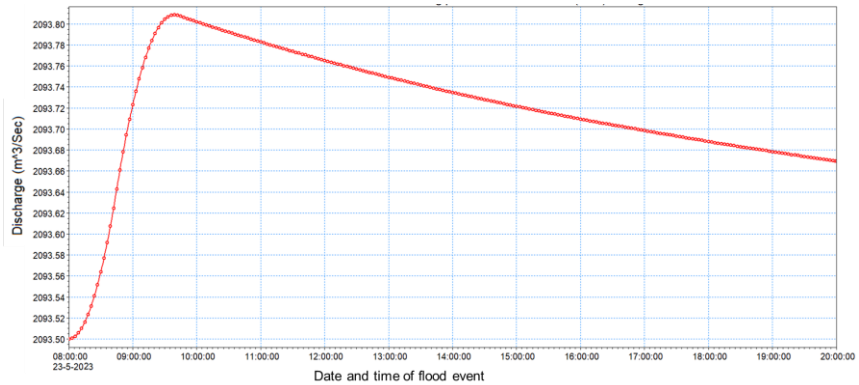


Figure 6. Time series of reservoir level during probable maximum flood (PMF) routing

2.7. Downstream flood inundation mapping

The methodology for downstream flood inundation mapping involved several key steps. Initially, the dam failure scenario was simulated using the MIKE Hydro River model, considering various breach parameters and hydraulic conditions. Once the dam breach was modeled, the resulting flood wave propagation downstream was simulated using the hydraulic model [91]. The downstream flood inundation mapping methodology included the delineation of flood extents based on water levels obtained from the hydraulic simulations. This involved overlaying the simulated water levels onto digital elevation models (DEMs) of the study area to identify areas prone to inundation.

2.8. Simulation of dam failure scenarios

In the context of assessing the potential impacts stemming from a dam failure event, the modeling endeavors focused on the evaluation of flood flow, depth, and velocity at specific locations along the river, particularly at two bridge sites [92, 93]. Through rigorous numerical simulations conducted within the framework of the dam failure modeling approach, the dynamics of flood propagation were comprehensively examined. This involved capturing the complex interactions between the released floodwaters and the natural and built environment surrounding the river corridor. Specifically, the flood flow characteristics, including flow rates and depth, were meticulously analyzed to understand the extent of inundation and the corresponding hydraulic

forces exerted on infrastructure such as bridges. Furthermore, the velocity of the floodwaters was scrutinized to gauge the intensity of flow and its potential impact on structural integrity and safety at the bridge locations.

Bridge-1, positioned at a longitudinal distance of 3241 meters along the river, traverses through a region characterized by a deep valley. Within this topographical context, minimal human habitation is observed until elevations surpass approximately 10 meters above the riverbed level. Conversely, **Bridge-2**, situated at a distance of 4128 meters along the river, marks a transition point where the river corridor widens, leading into a floodplain area that is habituated. The typical elevation of this floodplain area is recorded at approximately 1355 meters above sea level (Figure 4). Such delineation of the bridge locations based on the surrounding landscape and human settlement patterns provides crucial insights into the potential vulnerability of infrastructure and communities to flood hazards resulting from dam failure scenarios.

Multiple dam failure scenarios have been simulated, incorporating variations in breach widths and failure times. This approach allows for the exploration of a range of potential outcomes under different breach conditions, facilitating a comprehensive understanding of the associated flood dynamics and inundation extents resulting from dam failure events. Following the methodology outlined in Section 3.5, the modeling results are presented in the subsequent tables. These tables provide a detailed analysis of the simulated scenarios, allowing for an informed assessment of the implications and effectiveness of the applied modeling approach in capturing the dynamics of dam failure-induced flood events.

3. Results

3.1. Effect at bridge-1 (chainage 3241 m)

Among the dam failure scenarios simulated, the one yielding the greatest flood depths entails a breach width of 45 m and a failure time of 0.5 hours. In this scenario, the model predicts a peak water depth of 3.58 m, which stands approximately 3 meters below the level of habitation, alongside a peak velocity of 10.4 m/s. The corresponding time series of water level fluctuations is depicted in Figure 7 (A), providing a comprehensive visualization of the hydrodynamic dynamics over time (Table 6).

Table 6. Effect at Bridge-1 at chainage 3241 m

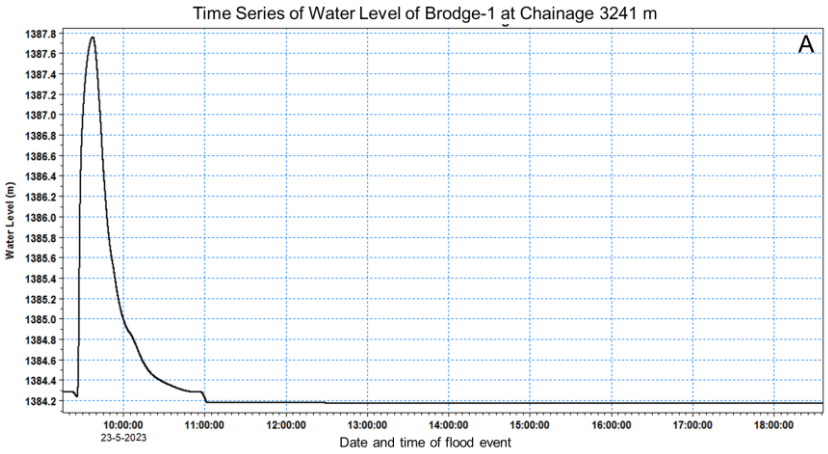
Average breach width (m)	Time of failure (hr)	Slope (H)	Breach level		Dam failure discharge (m^3/s)	Water level at bridge-1 (m, amsl)	Invert level at bridge-1 (m, amsl)
			Initial	Final			
20	0.5	1.0	2095.5	2076	858.52	1387.46	1384.19
	1				483.54	1386.83	
	2				260.34	1386.20	
	4				138.45	1385.76	
30	0.5	1.0	2095.5	2076	977.73	1387.72	
	1				526.64	1386.93	
	2				280.19	1386.26	
	4				147.51	1385.79	
45	0.5	1.0	2095.5	2076	1005.30	1387.76	
	1				540.10	1386.95	
	2				286.86	1386.28	
	4				150.50	1385.80	

3.2. Effect at bridge-2 (chainage 4128 m)

The dam breach scenario yielding the most substantial flood depths involves a breach width of 110 m and a failure time of 0.5 hours. In this scenario, the modeled peak water elevation reaches 1348.05 m, situated below habitation levels on both riverbanks. Concurrently, the peak velocity of the flood wave is recorded at 4.2 m/s. The hydrodynamic characteristics of this scenario are visually represented in Figure 7 (B), illustrating the propagation of the flood wave over time (Table 7).

Table 7. Effect at Bridge-2 at chainage 4128 m

Average breach width (m)	Time of failure (hr)	Slope (H)	Breach level (m)		Dam failure discharge (m^3/s)	Water level at bridge-2 (m, amsl)	Invert level at bridge-2 (m, amsl)
			Initial	Final			
20	0.5	1.0	2095.5	2076	858.52	1347.70	1343.98
	1				483.54	1346.98	
	2				260.34	1346.24	
	4				138.45	1345.65	
30	0.5	1.0	2095.5	2076	977.73	1348.08	
	1				526.64	1347.10	
	2				280.19	1346.32	
	4				147.51	1345.71	
45	0.5	1.0	2095.5	2076	1005.30	1348.05	
	1				540.10	1347.13	
	2				286.86	1346.34	
	4				150.50	1345.73	



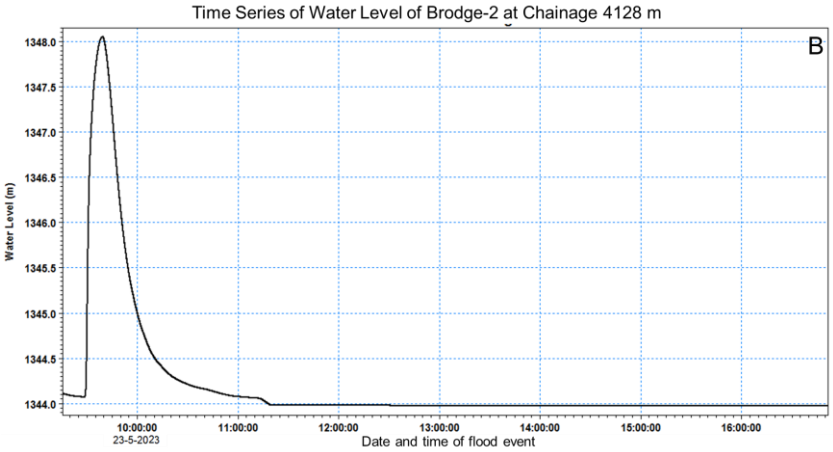


Figure 7. Time series of water level of (A) Brodge-1 at chainage 3241 m, and (B) Brodge-2 at chainage 4128 m.

3.3. Flood map

The flood maps provide a spatial interpretation of the model outputs derived from the one-dimensional simulations. In essence, the process involves interpolating the results from individual grid points across the grid space to construct comprehensive flood map. Flood map, depicted in Figure 8, encompass various land use categories such as settlement areas, cultivation land, and forested areas on GoogleEarth image. Such representations offer valuable insights into the extent and distribution of flood inundation across the study area, aiding in informed decision-making and disaster management efforts.

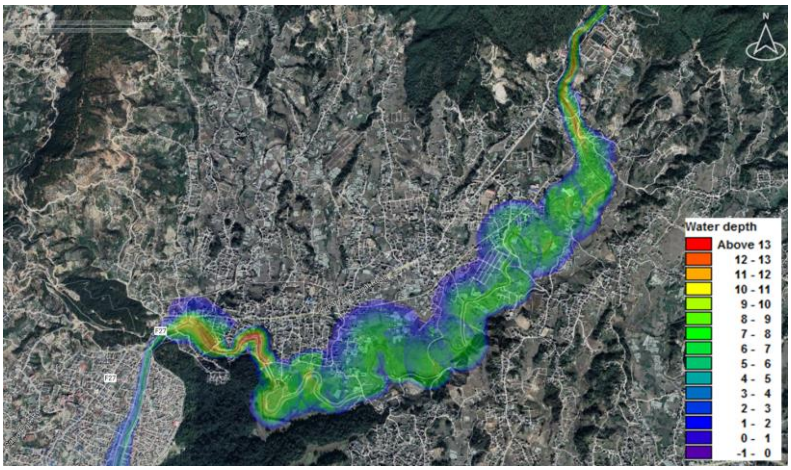


Figure 8. Flood map of model area, near Kathmandu metropolitan city.

The figures depicted in Figure 9 offer a two-dimensional representation derived from a one-dimensional model interpretation. Specifically, Figure 9 A and B illustrate flood maps corresponding to two specific locations along the river (chainage 3241 m and 4128 m). Within these maps, a red circle is employed to demarcate areas of impacted habitation. Notably, the

visualization indicates a limited number of habitations affected by the flood event, suggesting localized inundation. This observation underscores the significance of the flood mapping exercise in identifying specific areas prone to inundation and assessing the extent of habitat exposure to flood risks.

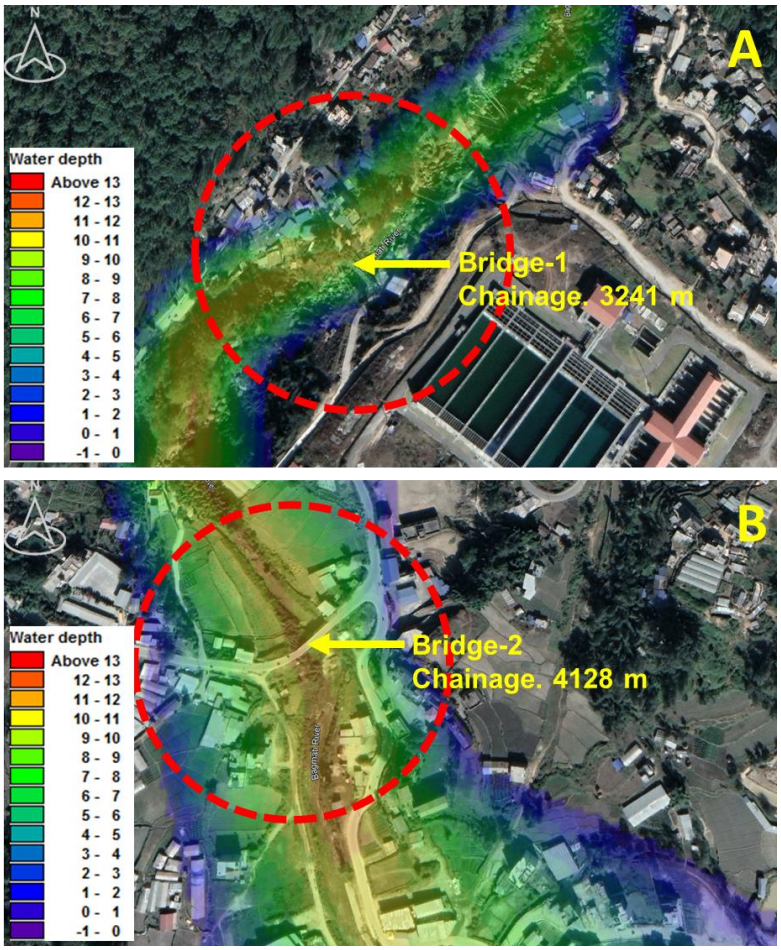


Figure 9. Flood map at (A) chainage 3241 m, and (B) chainage 4128 m.

3.4. Effect further downstream

The investigation delves deeper into the mechanism of flood peak attenuation, shedding light on the temporal dynamics of water level fluctuations. Figure 10 illustrates a series of time series depicting variations in water level over a specific period. The data showcased in the figure elucidate the process whereby the depth of the flood wave gradually diminishes, transitioning from an initial magnitude of 10 meters to a reduced level of 6 meters. This attenuation phenomenon underscores the inherent capacity of natural systems to mitigate the intensity of flood events over time, highlighting the role of hydraulic processes in regulating flood dynamics and minimizing the impact of inundation on vulnerable regions.

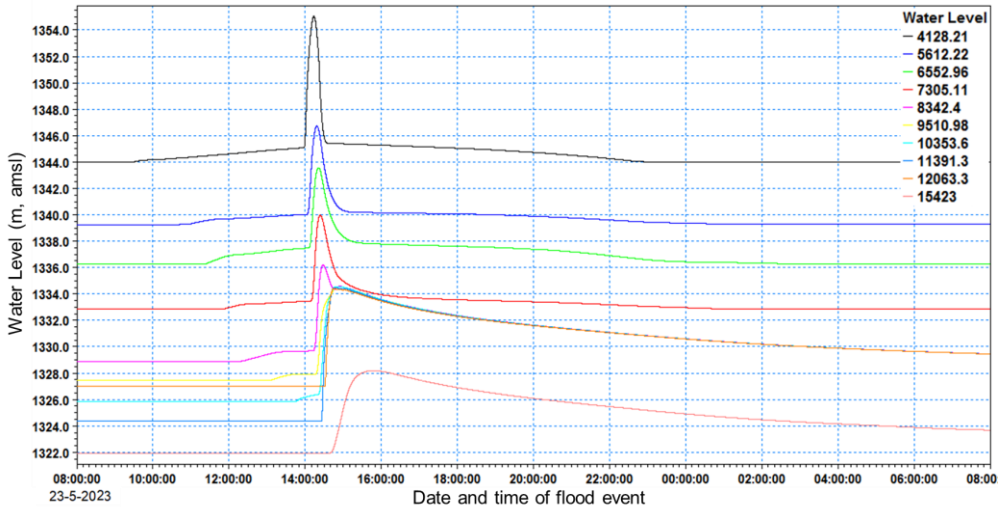


Figure 10. Flood wave attenuation at downstream of bridge (chainage 4128 m)

4. Conclusion

The integrated hydrodynamic modeling study in Kathmandu Valley, Nepal, utilized the MIKE Hydro River Model and diverse datasets including satellite imagery (Landsat-9 OLI-2, Sentinel-2), ALOS PALSAR RTC DEM data, topographical map at 1:25,000 scale, and hydraulic data to analyze flood dynamics. Sensitivity analysis of dam failure scenarios enhanced flood risk understanding and supported disaster management. Various scenarios, including the simulation of a probable maximum flood (PMF) routing, were conducted. The assessment focused on evaluating the impacts on infrastructure, specifically bridge-1 situated at chainage 3241m, and bridge-2 situated at chainage 4128m. Analysis revealed that the invert level at bridge-1 was determined to be 1384.19 m, whereas the invert level at bridge-2 was found to be 1343.98 m. Hydrodynamic modeling has emerged as a crucial tool in flood risk assessment, offering accurate simulations of water flow behavior and enabling informed decision-making for flood risk management and infrastructure resilience in vulnerable regions like Kathmandu metropolitan city. Historical data documents significant flood occurrences associated with this river across multiple years, encompassing 1988, 1991, 1995, 1996, 1999, 2018, 2019, 2021, 2022, and 2023. Historical data highlighted significant flood events from 1988 to 2023. Inundation modeling indicated river water levels of 13 meters near Gokarneshwar Mahadev, 8 meters near modeled bridges, and 5 to 6 meters elsewhere.

Hydrodynamic modeling holds significant implications for enhancing dam safety and flood management in Kathmandu metropolitan city. Through comprehensive assessments of dam safety and the creation of flood risk maps, authorities can effectively prioritize mitigation measures, formulate robust emergency response plans, and enact land use regulations to mitigate flood hazards. Furthermore, hydrodynamic modeling supports community awareness and facilitates the development of long-term adaptation strategies, promoting resilience and sustainable development practices in light of escalating flood risks. Addressing knowledge gaps through ongoing research endeavors, such as refining modeling techniques, integrating climate change scenarios, and adopting multi-hazard approaches, will further bolster flood risk assessment and management strategies. Ultimately, these efforts contribute to building resilience and reducing vulnerability in flood-prone regions like Kathmandu metropolitan city.

Funding statement

The author(s) received no financial support for the research, authorship, and/or publication of this article.

Authorship contribution statement

The author confirms being the sole contributor of this work and has approved it for publication.

Conflict of interest

The author reports no conflict of interest.

Acknowledgements

Author is grateful to Managing Director, DHI (India) Water & Environment Pvt Ltd, New Delhi, India for providing the necessary facilities to carry out this work.

References

1. Herschy, R.W. (2012). Dams and Reservoirs, Role. In L. Bengtsson, R.W. Herschy, & R.W. Fairbridge (Eds.), Encyclopedia of Lakes and Reservoirs. Encyclopedia of Earth Sciences Series. Springer, Dordrecht. https://doi.org/10.1007/978-1-4020-4410-6_155
2. Luixá-Sanmartín, J., Altarejos-García, L., Morales-Torres, A., & Escuder-Bueno, I. (2018). Climate change impacts on dam safety. Natural Hazards Earth System Sciences, 18, 2471–2488. https://doi.org/10.5194/nhess-18-2471-2018
3. DeNeale, S. T., Baecher, G. B., Stewart, K. M., Smith, E. D., & Watson, D. B. (2019). Current State-of-Practice in Dam Safety Risk Assessment. US Department of Energy, US. Retrieved from https://www.osti.gov/servlets/purl/1592163
4. Kenichiro, K., Zhongbo, Y., Guillermo, T.Q., Norlida, M.D., Ignasius, S.D.A., Yasuto, T., & Hans, T. (2021). Catalogue of hydrologic analysis for Asia and the Pacific, Volume 2: dam reservoir operation for addressing water related disasters, water scarcity and quality. UNESCO Intergovernmental Hydrological Programme. https://unesdoc.unesco.org/ark:/48223/pf0000380004
5. Kondolf, M., & Yi, J. (2022). Dam Renovation to Prolong Reservoir Life and Mitigate Dam Impacts. Water, 14(9), 1464. https://doi.org/10.3390/w14091464
6. Agonafir, C., Lakhankar, T., Khanbilvardi, R., Krakauer, N., Radell, D., & Devineni, N. (2023). A review of recent advances in urban flood research. Water Security, 19. https://doi.org/10.1016/j.wasec.2023.100141
7. Pakhale, G., Khosa, R., & Gosain, A. K. (2023). Are flood events really increasing? A case study of Krishna River Basin, India. Natural Hazards Research, 3(3), 374-384. https://doi.org/10.1016/j.nhres.2023.06.007
8. De Wrachien, D., & Mambretti, S. (2009). Dam-break Problems, Solutions and Case Studies. WIT Press, Southampton, Boston. Retrieved from https://www.witpress.com/images/stories/content_images/contents/c41429.pdf
9. Marcinkowski, P., & Grygoruk, M. (2017). Long-Term Downstream Effects of a Dam on a Lowland River Flow Regime: Case Study of the Upper Narew. Water, 9(10), 783. https://doi.org/10.3390/w9100783
10. Lyu, Z., Chai, J., Xu, Z., Qin, Y., & Cao, J. (2019). A Comprehensive Review on Reasons for Tailings Dam Failures Based on Case History. Advances in Civil Engineering. https://doi.org/10.1155/2019/4159306
11. Herbozo, J.E., Muñoz, L.E., Guerra, M.J., Minaya, V., Haro, P., Carrillo, V., Manciati, C., & Campozano, L. (2022). Non-Stationary Hydrological Regimes Due to Climate Change: The

Impact of Future Precipitation in the Spillway Design of a Reservoir, Case Study: Sube y Baja Dam, in Ecuador. Atmosphere, 13, 828. https://doi.org/10.3390/atmos13050828
12. Khosravi, K., Rostaminejad, M., Cooper, J. R., Mao, L., & Melesse, A. M. (2019). Dam break analysis and flood inundation mapping: The case study of Sefid-Roud Dam, Iran. In Extreme hydrology and climate variability (pp. 395-405). Elsevier. https://doi.org/10.1016/B978-0-12-815998-9.00031-2
13. Psomiadis, E., Tomanis, L., Kavvadias, A., Soulis, K. X., Charizopoulos, N., & Michas, S. (2021). Potential dam breach analysis and flood wave risk assessment using HEC-RAS and remote sensing data: A multicriteria approach. Water, 13, 364. https://doi.org/10.3390/w13030364
14. Ahmad, I., Waseem, M., Ashraf, A., et al. (2023). Hydrological risk assessment for Mangla Dam: compound effects of instant flow and precipitation peaks under climate change, using HEC-RAS and HEC-GeoRAS. SN Appl. Sci., 5, 344. https://doi.org/10.1007/s42452-023-05579-2
15. Paşa, Y., Peker, I. B., Hacı, A., & Gülbaz, S. (2023). Dam failure analysis and flood disaster simulation under various scenarios. Water Science and Technology, 87(5), 1214-1231. https://doi.org/10.2166/wst.2023.052
16. Awal, R. (2007). Study on landslide dam failure due to sliding and overtopping. Kyoto University. https://core.ac.uk/download/pdf/39199517.pdf
17. You, L., Li, C., Min, X., & Xiaolei, T. (2012). Review of dam-break research of earth-rock dam combining with dam safety management. Procedia Engineering, 28, 382–388. https://doi.org/10.1016/j.proeng.2012.01.737
18. Jiang, X., Meng, J., Fan, B., Zhao, C., Zheng, Y., Xiao, Q., Zhang, C., & Ma, D. (2023). Comparative analysis and risk assessment of dam-break floods: Taking Pingshuijiang Reservoir as an example. Hydrology Research, 54(2), 265–275. https://doi.org/10.2166/nh.2023.129
19. Costa, J. E., & Schuster, R. L. (1987). The formation and failure of natural dams. US Geological Survey Open-File Report 87-392, US Geological Survey, Vancouver, Washington. Retrieved from https://pubs.usgs.gov/of/1987/0392/report.pdf
20. Hancock, G. R., & Coulthard, T. J. (2022). Tailings dams: Assessing the long-term erosional stability of valley fill designs. Science of The Total Environment, 849. https://doi.org/10.1016/j.scitotenv.2022.157692
21. Shu, A., Wang, L., Zhu, F., Zhu, J., Pi, C., Zhang, Z., & Christian, H. (2022). Hydrodynamic process of partial and en masse dam failure induced debris flows. Frontiers in Environmental Science, 10, 905499. https://doi.org/10.3389/fenvs.2022.905499
22. Xu, F., Zhou, H., Zhou, J., & Yang, X. (2012). A mathematical model for forecasting the dam-break flood routing process of a landslide dam. Mathematical Problems in Engineering, 12. https://doi.org/10.1155/2012/139642
23. Prakash, M., Rothauge, K., & Cleary, P. W. (2014). Modelling the impact of dam failure scenarios on flood inundation using SPH. Applied Mathematical Modelling, 38(23), 5515-5534. https://doi.org/10.1016/j.apm.2014.03.011
24. Yang, Q., Guan, M., Peng, Y., & Chen, H. (2020). Numerical investigation of flash flood dynamics due to cascading failures of natural landslide dams. Engineering Geology, 276. https://doi.org/10.1016/j.enggeo.2020.105765
25. Korup, O., Strom, A., & Weidinger, J. (2006). Fluvial response to large rock-slope failures: Examples from the Himalayas, the Tien Shan, and the Southern Alps in New Zealand. Geomorphology, 78(3-4), 3-21. https://doi.org/10.1016/j.geomorph.2006.01.020

26. Pittman, J.M. (1917). Tigra Dam Failure, Gwalior, India-A Case of Sedimentary Sliding. Schnabel Engineering. Retrieved from https://damsafety.org/sites/default/files/Pittman%20Jonathan-decade%20dam.pdf
27. Rogers, J. D. (2006). Lessons learned from the St. Francis Dam failure. Geo-Strata, 2, 14-17. https://web.mst.edu/~rogersda/st_francis_dam/lessons_learned_from_the_st_francis_dam_failure(geostrata_mar-apr_2006).pdf
28. Moehne Dam. (1943). Bombing Moehne Dam Germany. https://caspir.warplane.com/eventdetail/eventid/3003000871943-05-17/
29. Duffaut, P. (2013). The traps behind the failure of Malpasset arch dam, France, in 1959. Journal of Rock Mechanics and Geotechnical Engineering, 5(5), 335-341. https://doi.org/10.1016/j.jrmge.2013.07.004
30. Nema, M. K., Mishra, P. K., & Jain, S. K. (2022). Dam decommissioning: An option for India's ageing water storage infrastructures. International Commission on Large Dams (INCOLD), New Delhi. http://www.incold.co.in/conf_2022/Papers/Dam%20decommissioning%20An%20option%20for%20India%E2%80%99s%20ageing%20water%20storage%20infrastructures.pdf
31. Ward, S. N., & Day, S. (2011). The 1963 landslide and flood at Vaiont reservoir Italy: A tsunami ball simulation. Italy Journal of Geoscience, 130(1), 16-26. https://websites.pmc.ucsc.edu/~ward/papers/Vaiont.pdf
32. Stava. (1985). The El Cobre Tailings dam failure, 1965. Stava. Retrieved from https://www.stava1985.it/the-el-cobre-disaster-chile/?lang=en
33. Carter, J. M., Williamson, J. E., & Teller, R. W. (1972). The 1972 Black Hills-Rapid City Flood Revisited. USGS Fact Sheet FS-037-02, U.S. Geological Survey, Rapid City, SD. Retrieved from https://pubs.usgs.gov/fs/fs-037-02/pdf/fs-037.pdf
34. Bai, S. N., & Zhen, Z. S. (2014). Study on the seepage defect at the connection of the overflow dam and the earth dam of Banqiao Reservoir. Advanced Materials Research, 3465, 287-291.
35. Arthur, H. G. (1977). Teton Dam Failure. In The Evaluation of Dam Safety: Engineering Foundation Conference Proceedings. ASCE, New York, New York, 61-71.
36. Solava, & Delatte. (2003). Teton Dam failure case study: Lessons from the failure of the Teton Dam. In Proceedings of the 3rd ASCE Forensics Congress, October 19 - 21, 2003, San Diego, California. Retrieved from https://faculty.washington.edu/kramer/521/TetonDamDescription.pdf
37. Coleman, N. M. (2018). Johnstown's Flood of 1889 - Power Over Truth and The Science Behind the Disaster. Springer International AG.
38. Luino, F., & Graff, J. V. D. (2012). The Stava mudflow of 19 July 1985 (Northern Italy): A disaster that effective regulation might have prevented. Natural Hazards Earth System Sciences, 12, 1029–1044. https://doi.org/10.5194/nhess-12-1029-2012
39. Simeoni, L., Tosatti, G., Lucchi, G., & Longo, M. (2017). The Stava catastrophic failure of 19th July 1985 (Italy): Technical-scientific data and socioeconomic aspects. Planning and Land Safety, Issue-1.
40. Reddy, D., Kumar, D., Saha, D., & Mandal, M. (2008). The 18 August 2008 Kosi River breach: An evaluation. Current Science, 95(12), 1668-1669.
41. Kafle, K.R., Khanal, S.N., & Dahal, R.K. (2017). Consequences of Koshi flood 2008 in terms of sedimentation characteristics and agricultural practices. Geoenviron Disasters, 4, 4. https://doi.org/10.1186/s40677-017-0069-x

42. Rautela, P. (2013). Lessons learnt from the deluge of Kedarnath, Uttarakhand, India. Asian Journal of Environment and Disaster Management (AJEDM), 5(2). https://rpsonline.com.sg/journals/101-ajedm/2013/0502/S1793924013002824.php
43. Allen, S. K., Rastner, P., Arora, M., Huggel, C., & Stoffel, M. (2015). Lake outburst and debris flow disaster at Kedarnath, June 2013: hydrometeorological triggering and topographic predisposition. Landslides. https://gaphaz.org/files/publications/allen_kedarnath_glof_landslides15.pdf
44. Lindell, M. K., Arlikatti, S., & Huangc, S. K. (2019). Immediate behavioral response to the June 17, 2013 flash floods in Uttarakhand, North India. International Journal of Disaster Risk Reduction, 34, 129–141. https://doi.org/10.1016/j.ijdrr.2018.11.011
45. ICIMOD. (2019). Learning from a disaster event: Investigating the 2018 Panjshir flood in Afghanistan. Mountain Environment Regional Information System. Retrieved from https://www.icimod.org/success-stories/learning-from-a-disaster-event-investigating-the-2018-panjshir-flood-in-afghanistan/
46. Rotta, L., Alcantara, E., Park, E., Negri, R., Lin, Y., Bernardo, N., & Mendes, T. (2020). The 2019 Brumadinho tailings dam collapse: Possible cause and impacts of the worst human and environmental disaster in Brazil. International Journal of Applied Earth Observation and Geoinformation, 90, 102119. https://doi.org/10.1016/j.jag.2020.102119
47. Cheng, D., Cui, Y., Li, Z., & Iqbal, J. (2021). Watch out for the Tailings Pond, a Sharp Edge Hanging over Our Heads: Lessons Learned and Perceptions from the Brumadinho Tailings Dam Failure Disaster. Remote Sensing, 13, 1775. https://doi.org/10.3390/rs13091775
48. Down-To-Earth. (2019). Ratnagiri dam breach: Flooding causes 44% of dam failures in India. Retrieved from https://www.downtoearth.org.in/news/water/throwback-how-china-s-sponge-cities-aim-to-re-use-70-of-rainwater-65399
49. BBC. (2021, February 8). Uttarakhand dam disaster: Race to rescue 150 people missing in India. BBC News. Archived from the original on February 9, 2021. Retrieved February 8, 2021.
50. NBC. (2023). Bodies wash ashore in Libya as devastated city races to count its dead. NBC News. Archived from the original on 2023-09-14. Retrieved 2023-09-14.
51. Johnson, F.A., & Illes, P. (1976). A Classification of Dam Failures. Waterpower and Dam Construction, 28(12), 43-45.
52. Singh, K. P., & Snorrason, A. (1982). Sensitivity of outflow peaks and flood stages to the selection of dam breach parameters and simulation models. University of Illinois, State Water Survey Division, Surface Water Section.
53. MacDonald, T. C., & Langridge-Monopolis, J. (1984). Breaching characteristics of dam failures. Journal of Hydraulic Engineering, 110(5), 567–586. https://doi.org/10.1061/(ASCE)0733-9429(1984)110:5(567)
54. Petra Check, A. W., & Sadler, P. A. (1984). Routing of dam break floods. International Waterpower & Dam Construction, 36, 29-32.
55. Singh, K. P., & Snorrason, A. (1984). Sensitivity of outflow peaks and flood stages to the selection of dam breach parameters and simulation models. Journal of Hydrology, 68(1-4), 295-310.
56. Froehlich, D. C. (1987). Embankment-Dam Breach Parameters. In Hydraulic Engineering, Proceedings of the 1987 National Conference, ASCE, Williamsburg, VA (pp. 570 - 575).
57. Wurbs, R. A. (1987). Dam breach flood wave models. Journal of Hydraulic Engineering, 113, 29-46.

58. Singh, V. P., Scarlatos, P. D., Collins, J. G., & Jaurdan, M. R. (1988). Breach erosion of earthfill dams (BEED) model. Natural Hazards, 1, 161-180.
59. Von Thun, J. L., & Gillette, D. R. (1990). Guidance on breach parameters. Unpublished internal document, U.S. Bureau of Reclamation, Denver, CO.
60. Dewey, R. L., & Gillette, D. R. (1993). Prediction of Embankment Dam Breaching for Hazard Assessment. In Proceedings, ASCE Specialty Conference on Geotechnical Practice in Dam Rehabilitation, Raleigh, North Carolina, April 25-28, 1993.
61. Horritt, M.S., & Bates, P.D. (2002). Evaluation of 1D and 2D Numerical Models for Predicting River Flood Inundation. Journal of Hydrology, 268, 87-99. https://doi.org/10.1016/S0022-1694(02)00121-X
62. Merritt, W. S., Letcher, R. A., & Jakeman, A. J. (2003). A review of erosion and sediment transport models. Environmental Modelling & Software, 18(8–9), 761-799. https://doi.org/10.1016/S1364-8152(03)00078-1
63. Yang, J., Townsend, R., & Daneshfar, B. (2006). Applying the HEC-RAS model and GIS techniques in river network floodplain delineation. Canadian Journal of Civil Engineering - CAN J CIVIL ENG, 33, 19-28. https://doi.org/10.1139/l05-102
64. Bani Hashemi et al. (2008). 2-dimension dam failure model by Fred and Mac Cormac approach. In 4th national conference of Civil Engineering, May 2008, University of Tehran, Iran. Retrieved from https://www.jmaterenvironsci.com/Document/vol6/vol6_N11/363-JMES-2015-Soleymani.pdf
65. Montazeri naming, et al. (2008). Simulation of the wave caused by dam failure through 1- and 2-dimension models; case study: Maroon Dam. In 4th National Conference of Civil Engineering, University of Tehran, Tehran.
66. Abareshi, M., Hosseini, S. M., & Jafarzade, M. R. (2010). Studying the risks of Taragh dam failure. In Fifth national conference of Civil Engineering, May 4-6, 2010, Ferdowsi University of Mashhad, Mashhad, Iran.
67. Esmaili, K., & Abbasi, B. (2010). Modeling of Dam Hydraulic Failure caused by sudden flood through Fluent software. In Fifth national conference of Civil Engineering, 4-6 May 2010, Ferdowsi University of Mashhad, Mashhad, Iran.
68. Ahmadi, & Toufani. (2011). Numerical modeling of dam gradual failure. In 6th national conference of Civil Engineering, April 26-27, 2011, Semnan University, Iran.
69. Timbadiya, P. V., Patel, P. L., & Porey, P. (2012). HEC-RAS based hydrodynamic model in prediction of stages of lower Tapi river. ISH Journal of Hydraulic Engineering, 17. https://doi.org/10.1080/09715010.2011.10515050
70. Godariz et al. (2013). Analyzing risk and uncertainty of earthen dam; case study: Doroudzan Dam in Fars province. Iran water research journal, fall and winter 2013, Shahr e- Kurd University.
71. Nejad, M., et al. (2014). Dam failure and its resulting wave propagation through using finite volume numerical method. Quarterly of Environment and Civil Engineering, University of Tabriz.
72. Seiyfi Zade et al. (2014). Studying Polroud dam failure caused by passing and flood routing at downstream. Research Journal of Watershed Management, Sciences and Natural Resources University, Sari.
73. Aureli, F., Dazzi, S., Maranzoni, A., Mignosa, P., & Vacondio, R. (2015). Experimental and numerical evaluation of the force due to the impact of a dam-break wave on a structure. Advances in Water Resources, 76, 29–42.

74. Kocaman, S., & Cagatay, H. (2015). Investigation of dam-break induced shock waves impact on a vertical wall. Journal of Hydrology, 525, 1–12. https://doi.org/10.1016/j.jhydrol.2015.03.048
75. Wood, A., & Wang, K. (2015). Modeling dam-break flows in channels with 90-degree bend using an alternating-direction implicit based curvilinear hydrodynamic solver. Computers & Fluids, 114, 254–264.
76. Dottori, F., Salamon, P., Bianchi, A., Alfieri, L., Hirpa, F. A., & Feyen, L. (2016). Development and evaluation of a framework for global flood hazard mapping. Advances in Water Resources, 94, 87–102. https://doi.org/10.1016/j.advwatres.2016.05.002
77. Vermee, S., Sachin, & Patra, K. C. (2022). Dam break flow simulation model for preparing emergency action plans for Bargi Dam failure. In R. Jha, V. P. Singh, V. Singh, L. B. Roy, & R. Thendiyath (Eds.), Hydrological modeling (Water Science and Technology Library, Vol. 109). Springer. https://doi.org/10.1007/978-3-030-81358-1_21
78. Palú, M. C., & Julien, P. (2020). Test and improvement of 1D routing algorithms for dam-break floods. Journal of Hydraulic Engineering, 146(6). https://doi.org/10.1061/(ASCE)HY.1943-7900.0001755
79. Li, C., Gao, H., Xu, Z., & Huang, Y. (2021). Sensitivity Analysis of Rock-Fill Dam Break Flood on Different Dam Break Durations. Open Journal of Safety Science and Technology, 11(3), 90-100. https://doi.org/10.4236/ojsst.2021.113008
80. Adityawan, M. B., Sandi, C., Harlan, D., Farid, M., Kuntoro, A. A., Widyaningtias, X. X., Chaidar, A. N., & Nugroho, J. (2023). Numerical modeling of dam break induced flow through multiple buildings in an idealized city. Results in Engineering, 18. https://doi.org/10.1016/j.rineng.2023.101060
81. Annunziato, A., Guney Dogan, G., & Yalciner, A. C. (2023). Modeling dam break events using shallow water model. Eng, 4, 1851-1870. https://doi.org/10.3390/eng4030105
82. DHI. (2023). MIKE HYDRO RIVER user guide. MIKE Powered by DHI. https://manuals.mikepoweredbydhi.help/latest/Water_Resources/MIKEHydro_River_UserGuide.pdf
83. HEC. (2014). Using HEC-RAS for Dam Break Studies, Training Document-39. U.S. Army Corps of Engineers, Hydrologic Engineering Center, 609 Second Street, Davis, CA. Retrieved from https://www.hec.usace.army.mil/publications/TrainingDocuments/TD-39.pdf
84. HEC. (1980, June). Flood Emergency Plans - Guidelines for Corps Dams, RD-13. U.S. Army Corps of Engineers, Hydrologic Engineering Center, 609 Second Street, Davis, CA. Retrieved from https://www.hec.usace.army.mil/confluence/rasdocs/ras1dtechref/latest/performing-a-dam-break-study-with-hec-ras/estimating-dam-breach-parameters/estimating-breach-parameters
85. USACE. (2007). HEC-ResSim-Reservoir system simulation, user's manual (Ver-3). U.S. Army Corps of Engineers, Hydrologic Engineering Center, 609 Second Street, Davis, CA. Retrieved from https://www.hec.usace.army.mil/Software/hec-ressim/documentation/HEC-ResSim_30_UsersManual.pdf
86. FERC. (1988, February 22). Notice of Revised Emergency Action Plan Guidelines. United States Federal Energy Regulatory Commission (FERC), USA. https://www.ferc.gov/sites/default/files/2020-04/02-22-88.pdf
87. Fread, D. L. (2006). Course notes on "Dam Break Floods". National Weather Service, NWS. U.S. Army Corps of Engineers, Hydrologic Engineering Center, 609 Second Street, Davis, CA.

88. Froehlich, D. C. (1995a). Embankment Dam Breach Parameters Revisited. In First International Conference, Water Resources Engineering, Environmental and Water Resources Institute (EWRD), 14 - 18 August 1995. ASCE, Water Resources Engineering Proceeding (pp. 887 - 891).
89. Froehlich, D. C. (1995b). Peak Outflow from Breached Embankment Dam. ASCE Journal of Water Resources Planning and Management, 121(1), 90 - 97.
90. Pareta K. 2023. Hydrological modelling of largest braided river of India using MIKE Hydro River software with rainfall runoff (RR), hydrodynamic (HD) and snowmelt modules. Journal of Water and Climate Change. Vol. 14(4), 1314, pp. 1-25. https://doi.org/10.2166/wcc.2023.484
91. Lompi, M., Mediero, L., Soriano, E., & Caporali, E. (2023). Climate change and hydrological dam safety: A stochastic methodology based on climate projections. Hydrological Sciences Journal, 68(6), 745-763. https://doi.org/10.1080/02626667.2023.2192873
92. Schultz, B. (2002). Role of Dams in Irrigation, Drainage and Flood Control. International Journal of Water Resources Development, 18(1), 147-162. https://doi.org/10.1080/07900620220121710
93. Xu, F., Yang, X., & Zhou, J. (2017). Dam-break flood risk assessment and mitigation measures for the Hongshiyan landslide-dammed lake triggered by the 2014 Ludian earthquake. Geomatics, Natural Hazards and Risk, 8(2), 803-821. https://doi.org/10.1080/19475705.2016.1269839

© 2024 by the authors. Licensee SCU, Ahvaz, Iran. This article is an open access article distributed under the terms and conditions of the Creative Commons Attribution 4.0 International (CC BY 4.0 license) (http://creativecommons.org/licenses/by/4.0/).